High frequency electron paramagnetic resonance spectroscopy of nitroxide-functionalized nanodiamonds in aqueous solution

R. D. Akiel, V. Stepanov, and S. Takahashi^{1,2,*}

¹Department of Chemistry, University of Southern California, Los Angeles CA 90089, USA

²Department of Physics and Astronomy, University of Southern California, Los Angeles CA 90089, USA

* E-mail: susumu.takahashi@usc.edu

Keywords: Electron paramagnetic resonance, High frequency, Aqueous sample, Nanodiamond, Nitroxide, Click chemistry

Abstract

Nanodiamond (ND) is an attractive class of nanomaterial for fluorescent labeling, magnetic sensing of biological molecules, and targeted drug delivery. Many of those applications require tethering of target biological molecules on the ND surface. Even though many approaches have been developed to attach macromolecules to the ND surface, it remains challenging to characterize dynamics of tethered molecule. Here, we show high-frequency electron paramagnetic resonance (HF EPR) spectroscopy of nitroxide-functionalized NDs. Nitroxide radical is a commonly used spin label to investigate dynamics of biological molecules. In the investigation, we developed a sample holder to overcome water absorption of HF microwave. Then, we demonstrated HF EPR spectroscopy of nitroxide-functionalized NDs in aqueous solution and showed clear spectral distinction of ND and nitroxide EPR signals. Moreover, through EPR spectral analysis, we investigate dynamics of nitroxide radicals on the ND surface. The demonstration sheds light on the use of HF EPR spectroscopy to investigate biological molecule-functionalized nanoparticles.

Introduction

Nanoparticles are emerging materials revolutionizing many fields including biology, chemistry, materials science, medicine and physics. Among nanoparticles, nanodiamond (ND) has recently been investigated extensively because of their physical and chemical stability and biocompatibility. In addition, in a majority of cases, NDs contain nitrogen-vacancy (NV) centers, which are atomic-scale fluorescent defects with excellent quantum properties. Thus, ND is a promising material for applications of biological imaging, targeted drug delivery and nano-scale sensing (1-13). In many of those applications, functional biological molecules need to be tailored to the ND surfaces. Even though many approaches to attach biological molecules to ND surfaces have been investigated (5, 8, 12, 14-16), it remains challenging to monitor behaviors of the grafted molecules because the presence of ND hampers the employment of standard techniques (e.g., chromatography and optical spectroscopy).

Electron paramagnetic resonance (EPR) spectroscopy is a powerful technique to probe spin states and dynamics of unpaired electrons. EPR spectroscopy is widely used to investigate dynamical behaviors and microenvironments of various molecules including free radicals and biological molecules (17-19) In particular, for investigation of biological molecules, site-directed spin labeling (SDSL) has been developed to introduce a spin probe at a specific site within macromolecule (20, 21). Investigation using SDSL and EPR spectroscopy has been performed in many biological systems including proteins (T4-lysozyme (19, 22), rhodopsin (23), bacterirhodopsin (19, 24), proteorhodopsin (25) etc), DNAs and RNAs (26). Nitroxide radical is the most common spin label used in SDSL. Nitroxide radical containing a stable and unpaired electron consists of five or six membered rings containing a nitroxyl group surrounded by four methyl groups that are attached to adjacent carbons. The unpaired electron in nitroxide radical occupies a π -orbital that is delocalized over the nitrogen and the oxygen atoms, thus making its

EPR g-values and hyperfine-coupling constants highly anisotropic (27). EPR analysis of nitroxide radicals is a powerful tool to probe the dynamics of the molecules and their local environments because the EPR spectrum representing their g-values and hyperfine couplings drastically changes with the degree of the molecular dynamics, characterized by the rotation correlation time (τ_c). In the case of nitroxide radicals grafted on a nanoparticle, the correlation time is influenced by tumbling motions of the nanoparticles and side-chain motions of the nitroxide molecules.

In this work, we employ 230 GHz and 115 GHz EPR spectroscopy to study dynamics of nitroxide-functionalized NDs in solution. High-frequency (HF) EPR spectroscopy is highly advantageous to distinguish EPR signals of nitroxide radicals and NDs because of its high spectral resolution. For the HF EPR investigation, we develop a sample holder for aqueous solution samples to overcome water absorption of HF microwave. Using the sample holder, we perform HF EPR spectroscopy of 2,2,6,6-tetramethylpiperidine-1-oxyl (TEMPO) radicals covalently attached to NDs where the grafted TEMPO is positioned ~1.8 nm away from the ND surface. We show that HF EPR spectroscopy allows the distinction of EPR signals between ND and the nitroxide radicals spectrally. Furthermore, we perform EPR analysis of the obtained spectrum to investigate dynamics of nitroxide radicals.

Materials and methods

Nanodiamonds

The NDs used in this work were produced by high-pressure-high-temperature (HTHP) process with an average size of 100 nm (Engis, Inc.). HPHT diamond is classified as type-Ib diamonds. Common paramagnetic impurities in HPHT diamond are nitrogen-related impurities whose concentration is typically in the order of 10 to 100 parts per million (ppm) carbon atoms. For the covalent attachment of nitroxide radicals on the ND surface, NDs were functionalized with azide

groups using the salinization techniques. First, NDs were acid treated to increase the number of carboxyl groups on their surface and remove any graphitic or metallic impurities. Second, the NDs were subjected to borane-reduction to transform the carboxyl groups into hydroxyl groups which were reacted with 3-bromopropyltrichlorosilane to yield bromine groups. Finally, the bromine group was substituted with an azide (-N₃) group to obtain azide functionalized NDs (N₃-ND) (see Ref. (28) for the details of the functionalization).

Nitroxide radicals grafted on the nanodiamond surface

Nitroxide radicals studied here were covalently attached on the ND surface. The nitroxide was attached to the surface of the ND using copper free click reaction. In copper free click reaction, we employed succinimide-amine chemistry to add a dibenzocyclooctyne (DBCO) moiety to a 1-oxyl-2,2,6,6-tetramethylpiperidine (TEMPO) radical. Then, without further purification, the mixture containing DBCO functional TEMPO (TEMPO-DBCO) was added to 0.3 mg N₃-NDs. The reaction mixture was ultrasonicated overnight. Finally, the resulting NDs (TEMPO-NDs) were purified by repeated washing with acetonitrile followed by centrifugation until no free TEMPO was detected in the supernatant by EPR spectroscopy (see Ref. (29) for detailed method).

230 GHz/115 GHz EPR spectroscopy

The 230 GHz/115 GHz EPR system employs a high-power solid-state source consisting of 8–10 GHz synthesizer, PIN switch, microwave amplifiers, and frequency multipliers. The output power of the source system is 100 mW at 230 GHz and 700 mW at 115 GHz. The 230 GHz/115 GHz excitation is propagated using quasioptical bridge and a corrugated waveguide, and couples to a sample located at the center of a 12.1 T, cryogenic-free, superconducting magnet. EPR signals are isolated from the excitation using an induction mode operation. For EPR detection, the system employs a superheterodyne detection system in which 230 GHz or 115 GHz is down-converted

into 3 GHz of intermediate frequency (IF), which is then down-converted again to in-phase and quadrature components of DC signals. (see Ref. (30, 31) for details of the system). The microwave power and magnetic field modulation strength were adjusted to maximize the intensity of EPR signals without distorting the lineshape (typically, the microwave power is 2 mW and the modulation amplitude is 0.1 mT with modulation frequency of 20 kHz).

X-band EPR spectroscopy

X-band cw EPR spectroscopy was performed using the Bruker EMX system (Bruker Biospin) equipped with a high-sensitivity cavity (ER 4119HS, Bruker Biospin). For each measurement, samples were placed in a quartz capillary (inner diameter: 0.86 mm), with the typical sample volume being 1–5 μL. cw EPR spectra were obtained by optimizing the microwave power and magnetic field modulation strength to maximize the amplitude of EPR signals without distorting the lineshape, with a typical parameter set being: microwave power of 2 mW; modulation amplitude of 0.03 mT; and modulation frequency of 100 kHz.

Results and Discussions

Design of the sample holder for EPR measurement of aqueous samples at 115 GHz

While HF EPR is advantageous for high spectral resolution, a large amount of water absorption of HF microwave often challenges the implementation of HF EPR experiments at physiological conditions, *i.e.* room temperature aqueous samples. In particular, the absorption is significant at 0.1 - 1 THz. (32). For example, 1 mm thickness of water absorbs 10 % of microwave power at 10 GHz while at 115 GHz it absorbs 99.98 %. As demonstrated in Ref. (33), one way to overcome the water absorption of HF microwave is to employ a thin layer of the aqueous sample where the thickness of the layer (h) is much smaller than the microwave wavelength (λ). As shown in Figure 1a, the magnetic component of the microwave (B_1) is maximum at a conducting surface (i.e.

aluminum tape) while the electric component of the microwave (E_1) is minimum. This allows to "mask" thin aqueous samples from the electric field, resulting in reduction of the microwave absorption.

To implement this idea for our HF EPR system, we designed a sample holder as shown in Figure 1b. The sample holder made of Teflon is designed to hold an aqueous sample in a cylindrical well (Figure 1b). In the present design, the sample holder is used with no microwave cavity and aqueous sample solution is placed on a conducting surface which is the node of the microwave electric component as well as the antinode of the magnetic component (Figure 1a). To minimize the microwave absorptions and to maximize the sample volume, the well height (h) was chosen to be ~100 μ m and the well diameter (D) is ~5 mm where D is similar to the aperture of the corrugated waveguide. The sample well is sealed by an aluminum tape. Moreover, the sample well is located at a distance (d) from the corrugated waveguide that satisfies the condition $dn_T + hn_W = 2\lambda$ where n_T – refraction index of Teflon (n_T = 1.44), n_W – refraction index of water (n_W = 1.33) and λ – microwave wavelength at 115 GHz.

Paramagnetic impurities in NDs

Figure 2 shows continuous-wave (cw) 230 GHz EPR spectrum of the 100 nm-ND sample. cw EPR spectrum was obtained from a dry powder of NDs. The ND sample was placed in a Teflon sample holder (5 mm diameter) with the volume of 1 μ L. The obtained 230 GHz EPR spectrum shows two kinds of EPR signals which are well-understood by considering the substitutional single nitrogen impurity (N spins, also known as P1 centers) and the S=1/2 surface impurity in diamond (28). N spins are well-characterized paramagnetic impurities within the diamond lattice (S = 1/2, I = 1, $g_{x,y} = 2.0024$, $g_z = 2.0024$, and the ¹⁴N hyperfine coupling $A_x = A_y = 82$ MHz, $A_z = 114$ MHz).

The surface S = 1/2 paramagnetic impurities were also observed previously $(g_{x,y} = 2.0029 \pm 0.0001)$ and $g_z = 2.0027 \pm 0.0001)$ (28).

Nitroxide grafted on NDs through copper free click reaction

Here we discuss EPR analysis of nitroxide radicals grafted on the ND surface. First, Figure 3a shows 115 GHz EPR spectrum of the 100 nm N₃-ND sample. The spectrum shows a signal from 4.098 Tesla to 4.108 Tesla (Figure 3a, blue). To confirm that the observed signal corresponds to the paramagnetic impurities in the diamond, we simulated EPR spectrum using the same parameters described above. As shown in Figure 3a, we showed that the simulated result of ND EPR spectrum agreed reasonably well with the experimental data (Figure 3a, red), which confirms that the azide functionalization does not change the EPR of NDs as we expect. Moreover, the N₃-ND sample was measured by X-band EPR spectrometer. As shown in Figure 3b, the two EPR signals largely overlapped because of the small difference in their g-values. The obtained EPR data showed a prominent signal at ~0.3328 Tesla and two other signals at ~0.3300 Tesla and ~0.3357 Tesla (Figure 3b, blue). Using the same parameters and following the same procedure as the HF EPR analysis, we demonstrated that the simulated X-band spectrum of N₃-ND (Figure 3b, green) agreed with the experimental results too.

After functionalizing the ND with nitroxide radicals (29), HF EPR and X-band EPR were measured for the product (TEMPO-ND). As shown in Figure 4a, HF EPR spectrum of the TEMPO-ND sample was different from ND EPR spectrum (Figure 3a) and showed a distinct signal at around 4.095 Tesla in addition to the ND signals (Figure 4a, blue). In addition, we also performed X-band EPR measurement of the TEMPO-ND sample. As shown in Figure 4b, the TEMPO-ND spectrum is represented by a broad peak at 0.3325 Tesla. When nitroxide radicals are free in solution, a fast rotational tumbling of the molecules ($\tau_c = 0.03$ ns) averages out the g- and

A-anisotropies, and the EPR spectrum is dominated by isotropic hyperfine coupling. Consequently, the EPR spectrum appears as three signals of comparable intensities as shown in Figure 4c. When $τ_c$ of nitroxide radicals increase due to slower rotational motions, it causes different degrees of the averaging which will translate into spectral broadening and uneven changes of the EPR signal intensities. Furthermore, we estimated the amount of TEMPO loaded on the surface of ND by analyzing the intensity of the obtained signal. By comparing the intensity of the simulated TEMPO (Figure 4b, magenta) with that of known concentrations, the number of TEMPO on ND surface was estimated to be 0.05 nmol, corresponding to $3x10^{13}$ molecules. Giving a density of ND of 3.51 g/cm³ and ~5.2 × 10^{-16} cm³ for the volume of one 100-nm diameter spherical ND, the number of ND particles in the measured sample was estimated to be ~5.5×10¹⁰. Thus, the surface load of TEMPO was estimated ~550 TEMPO molecules for each ND particle.

To verify the EPR signals of TEMPO grafted on the ND surface, we performed EPR spectrum analysis of the TEMPO-ND sample. In the analysis, we took into account the simulated result of ND (Figure 4a, green) and simulated EPR spectrum of TEMPO radicals (S = 1/2, I = 1, $g_x = 2.0086$, $g_y = 2.0056$, $g_z = 2.0033$, $A_x = 6.5$, $A_y = 5.6$, $A_z = 37$ MHz) (Figure 4a, magenta). By combining those EPR signals (Figure 4a, red), we found a good agreement between the experimental data and the simulation with the TEMPO spectrum. From the analysis, we obtained that the correlation time of TEMPO on the ND surface is $\tau_c = 4.1$ ns. Moreover, X-band EPR of the TEMPO-ND sample was also performed. Although X-band EPR spectrum of the TEMPO-ND sample showed that EPR signal of TEMPO at ~0.3308 Tesla largely overlaps with the ND spectrum (Figure 4b, blue), we found a good agreement between the observed X-band spectrum and the simulation using the parameters obtained from the HF EPR analysis (Figure 4b, red). Therefore, the result confirms the observation of EPR signals of TEMPO grafted on the ND surface. As seen in Figure 4b and c, the

EPR spectrum of the TEMPO grafted on the ND surface was much broader than that of the free TEMPO sample because of the slower correlation time. The simulation of the EPR spectrum was done using the Easyspin's slow-motion function which simulates EPR spectrum by calculating the spin dynamics with the Stochastic-Liouville equation formalism (34-39).

When TEMPO is tethered to the ND surface, two modes of motion contribute to the dynamics of the nitroxide radical. The first one is the rotational tumbling of the TEMPO which is greatly affected by the rotational tumbling of the ND particle itself (Figure 5i). The second one is the rotation of the TEMPO molecule that is allowed due to four torsional rotational motion about the bonds that links the nitroxide to the nanoparticle, called internal motion (Figure 5ii). By modeling the rotational tumbling of ND by rotational diffusion of a spherical particle, the rotational correlation time of the 100 nm ND is given by the Stocks-Einstein-Debye equation (40):

$$\tau_c = \frac{V_h \eta}{k_B T} \tag{1}$$

where $k_{\rm B}$ is the Boltzmann constant, T is the sample temperature, η is the viscosity of water ($\sim 8.9 \times 10^{-4}~{\rm J~s/m^3}$), and $V_{\rm h}$ is the hydrodynamic volume ($\sim 5.2 \times 10^{-22}~{\rm m^3}$). Using Equation (1), we estimated the rotational correlation time of 100 nm-NDs to be 113 μs . This correlation time is much slower than the observed τ_c , thus the observed EPR spectrum is dictated solely by the internal motion of TEMPO. Furthermore, the slower correlation time ($\tau_c = 4.1~{\rm ns}$) than that of the free nitroxide suggests that the internal motion of the nitroxide molecule is greatly slowed down due to the short and solid C-C linkers connecting it to ND ($\sim 1.8~{\rm nm}$ distance between TEMPO and ND surface).

Conclusion

In this work, we used HF EPR spectroscopy to investigate motions of nitroxide radicals grafted on the ND surface. Using the HF EPR, we demonstrated to spectrally separate EPR signals of NDs

and nitroxide radicals. In addition, we showed the investigation of dynamics of nitroxide radicals through EPR spectral analysis. The investigation sheds light on the use of HF EPR spectroscopy to investigate dynamics of biological molecules grafted on the surface of nanoparticles.

Acknowledgment

This work was supported by the Searle Scholars Program, the USC Anton B. Burg Foundation and the National Science Foundation (DMR-1508661) (S.T.).

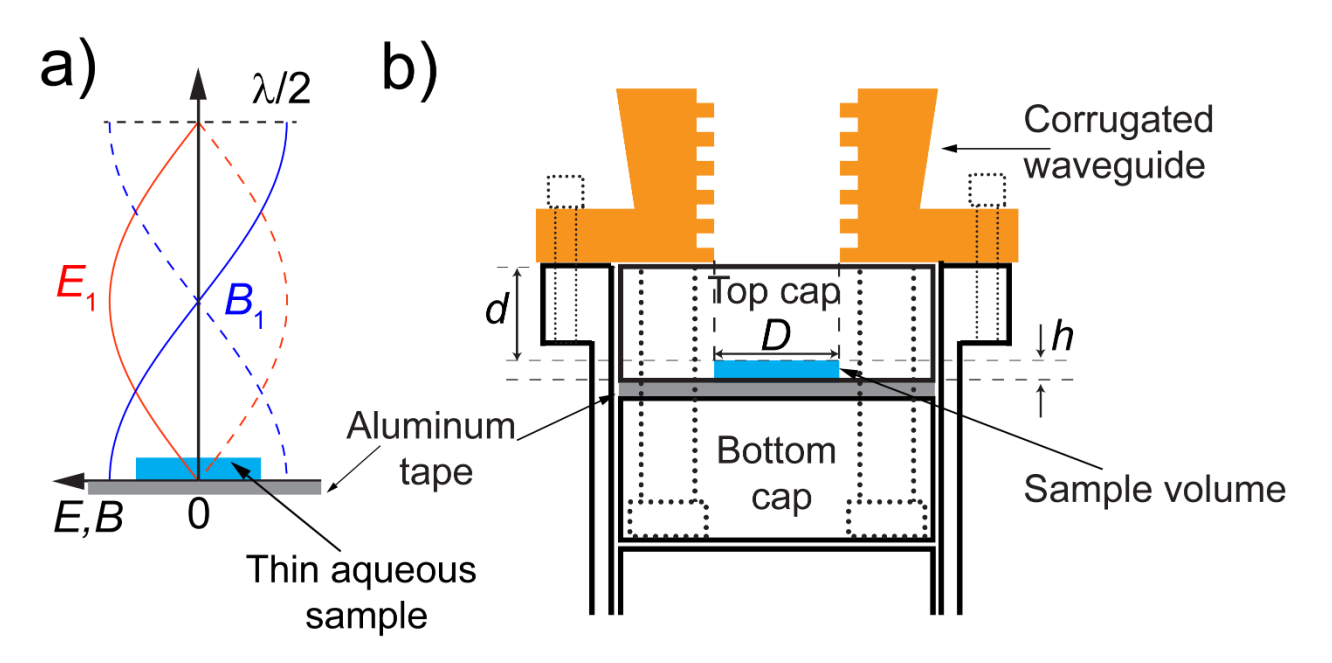


Figure 1. Aqueous sample holder. a) Electric and magnetic field components of microwave in the sample holder. The sample is positioned on the aluminum tape. b) Schematics for aqueous sample design. The top and bottom caps are made of Teflon. Doted lines indicate threads and volume for screws that are used to tighten top and bottom caps.

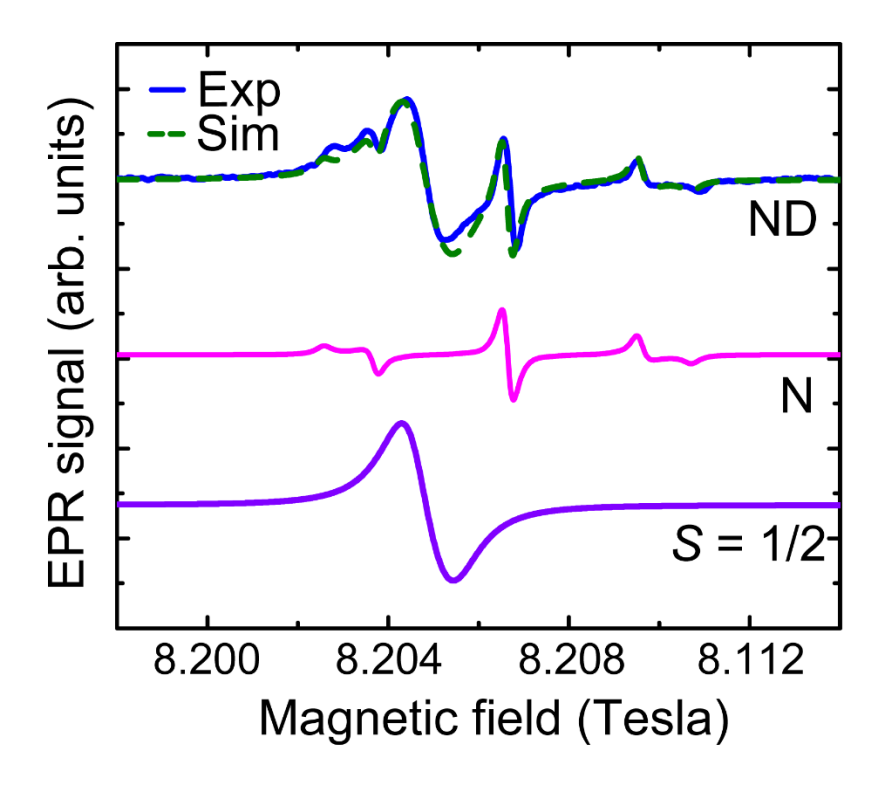


Figure 2. Spectral analysis of 100 nm-ND EPR signals. 230 GHz EPR of the NDs is shown by the solid blue line. The spectrum of the N spins was simulated using S = 1/2, I = 1, $g_{x,y} = 2.0024$, $g_z = 2.0024$, and the ¹⁴N hyperfine coupling $A_x = A_y = 82$ MHz, $A_z = 114$ (magenta). S = 1/2 spins was simulated with S = 1/2, $g_{x,y} = 2.0029 \pm 0.0001$ and $g_z = 2.0027 \pm 0.0001$ (violet). The green dotted line is the sum of the N and S = 1/2 EPR spectra. The simulations were performed using Easyspin (41).

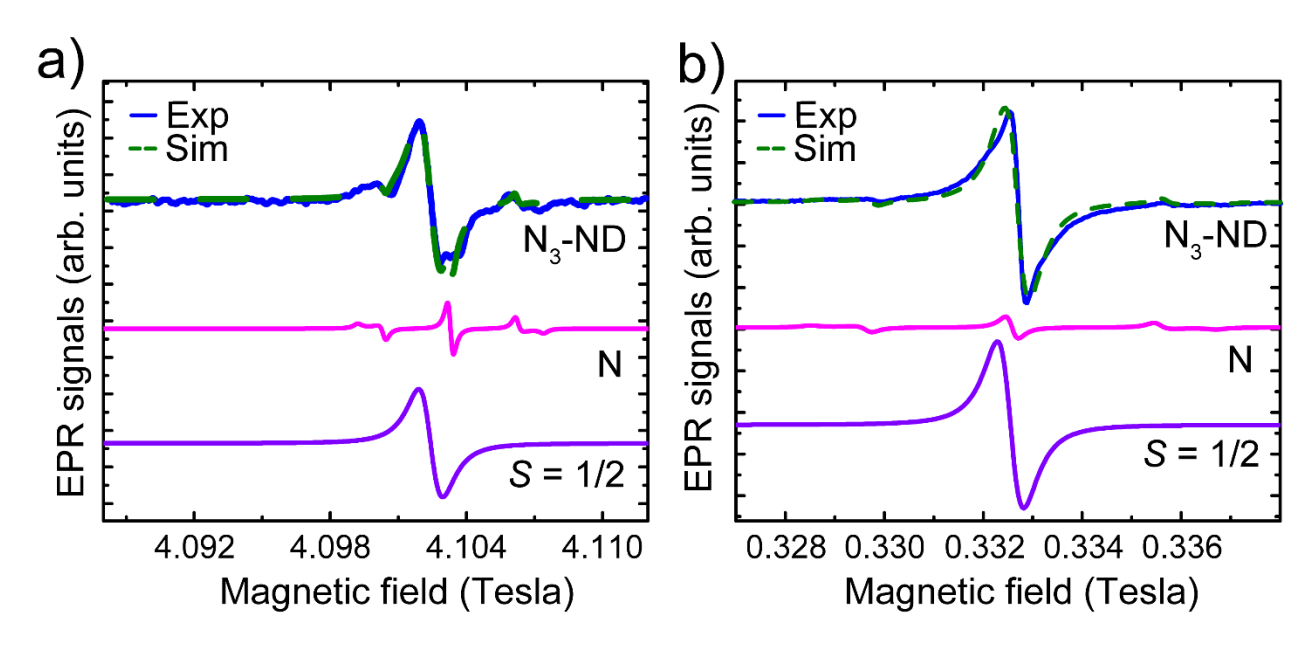


Figure 3. EPR analyses of the N₃-ND sample. a) 115 GHz EPR of N₃-ND and b) X-band EPR of N₃-ND are shown by the solid blue lines. a) and b) also show the contributions of N (magenta) and the S = 1/2 spins (purple) obtained by simulating the experimental EPR spectra. The dotted green lines overlaid with the experimental data shows the sum of the N and S = 1/2 contributions. The simulations were performed using Easyspin (41).

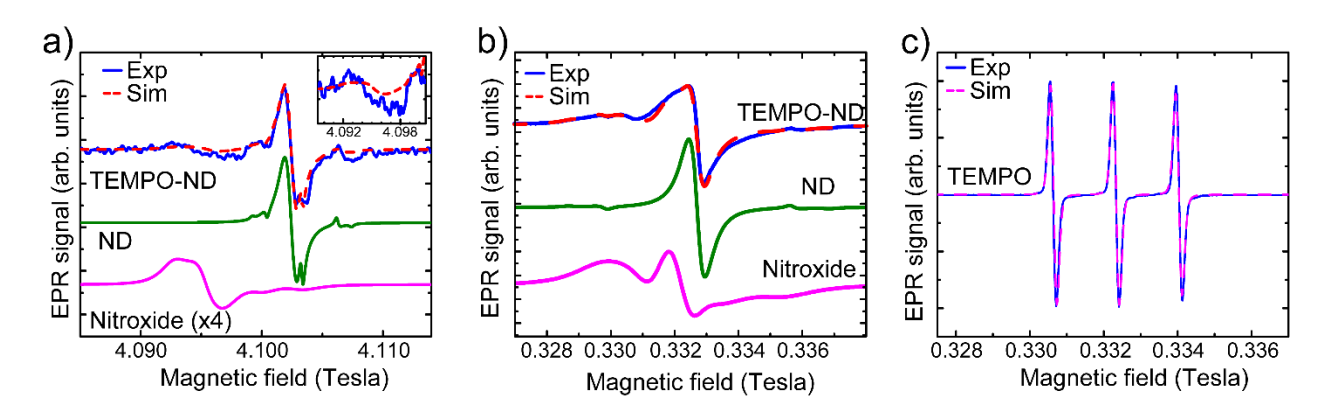


Figure 4. EPR analyses of the TEMPO-ND sample. a)115 GHz EPR data. The experimental EPR data of nitroxide radicals is magnified by 4 times. The solid blue line is experimental data, and the green and magenta solid lines are simulated EPR spectra of ND and nitroxide radical. The red dotted line shows the sum of the simulated spectra. b) X-band EPR data are shown by the solid blue lines. The green and magenta solid lines show the contributions of ND and nitroxide EPR signals. The sum of the ND and nitroxide signals is shown by the red dotted lines. Note that samples in a) and b) were suspended in phosphate-buffered saline pH 7 at a concentration of 0.1 mg/ μ L and the spectra were recorded at room temperature. c) X-band EPR spectrum of free nitroxide in aqueous solution. The simulated spectrum is shown by the magenta dotted line. The simulations were performed using Easyspin (41).

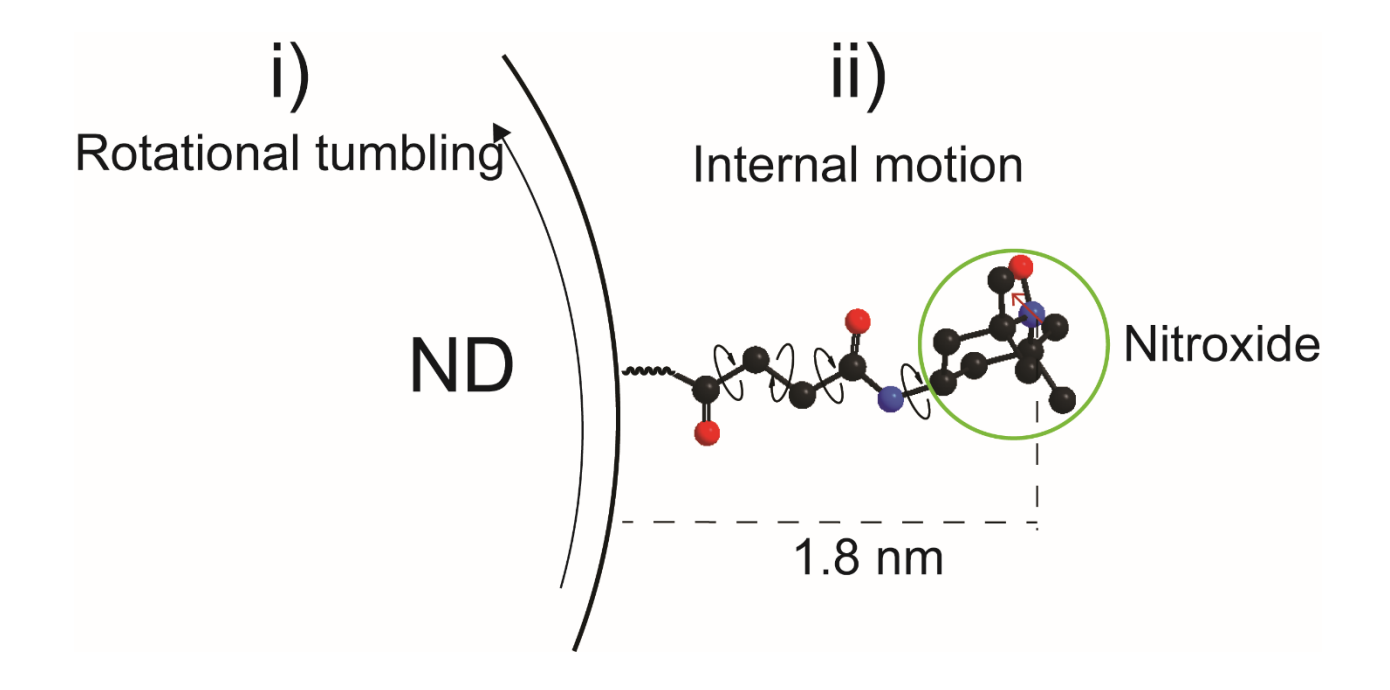


Figure 5. Motions of grafted nitroxide radical. i) Global rotational tumbling of ND. ii) Internal motion of nitroxide radical.

References

- Balasubramanian G, Chan I Y, Kolesov R, Al-Hmoud M, Tisler J, Shin C, Kim C, Wojcik A, Hemmer P R, Krueger A, Hanke T, Leitenstorfer A, Bratschitsch R, Jelezko F, Wrachtrup J (2008) Nanoscale imaging magnetometry with diamond spins under ambient conditions. Nature. 2008. 455, 648-651.
- 2. Maze J R, Stanwix P L, Hodges J S, Hong S, Taylor J M, Cappellaro P, Jiang L, Dutt M V G, Togan E, Zibrov A S, Yacoby A, Walsworth R L, Lukin M D (2008) Nanoscale magnetic sensing with an individual electronic spin in diamond. Nature. 2008. 455, 644-647.
- 3. Degen C L (2008) Scanning magnetic field microscope with a diamond single-spin sensor. Appl. Phys. Lett. 2008. 92, 243111.
- 4. Taylor J M, Cappellaro P, Childress L, Jiang L, Budker D, Hemmer P R, Yacoby A, Walsworth R, Lukin M D (2008) High-sensitivity diamond magnetometer with nanoscale resolution. Nat. Phys. 2008. 4, 810-816.
- 5. Chang B-M, Lin H-H, Su L-J, Lin W-D, Lin R-J, Tzeng Y-K, Lee A T, Lee Y C, Yu A L, Chang H-C (2013) Highly fluorescent nanodiamonds protein-functionalized for cell labeling and targeting. Adv. Funct. Matter. 2013. 23, 5737-5745.
- 6. Fu C-C, Lee H-Y, Chen K, Lim T-S, Wu H-Y, Lin P-K, Wei P-K, Tsao P-H, Chang H-C, Fann W (2007) Characterization and application of single fluorescent nanodiamonds as cellular biomarkers. Proc. Natl. Acad. Sci. 2007. 104, 727-732.
- 7. Holt K B (2007) Diamond at the nanoscale: applications of diamond nanoparticles from cellular biomarkers to quantum computing. Phil. Trans. R. Soc. A. 2007. 365, 2845-2861.
- 8. Huang L ,Chang H-C (2004) Adsorption and immobilization of cytochrome c on nanodiamonds. Langmuir. 2004. 20, 5879-5884.
- 9. Krueger A, Liang Y, Jarre G, Stegk J (2006) Surface functionalisation of detonation diamond suitable for biological applications. J. Mater. Chem. 2006. 16, 2322.
- McGuinness L P, Yan Y, Stacey A, Simpson D A, Hall L T, Maclaurin D, Prawer S, Mulvaney P,
 Wrachtrup J, Caruso F, Scholten R E, Hollenberg L C L (2011) Quantum measurement and

- orientation tracking of fluorescent nanodiamonds inside living cells. Nat. Nanotechnol. 2011. 6, 358–363.
- 11. Wenga M-F, Changa B-J, Chianga S-Y, Wang N-S, Niuc H (2012) Cellular uptake and phototoxicity of surface-modified fluorescent nanodiamonds. Diamond Relat. Mater. 2012. 22, 96-104.
- 12. Zhao L, Nakae Y, Qin H, Ito T, Kimura T, Kojima H, Chan L, Komatsu N (2014) Polyglycerol-functionalized nanodiamond as a platform for gene delivery:Derivatization, characterization, and hybridization with DNA. J. Org. Chem. 2014. 10, 707-713.
- 13. Kaur R ,Badea I (2013) Nanodiamonds as novel nanomaterials for biomedical applications: drug delivery and imaging systems. Int. J. Nanomedicine. 2013. 8, 203-220.
- 14. Ermakova A, Pramanik G, Cai J-M, Algara-Siller G, Kaiser U, Weil T, Tzeng Y-K, Chang H C, McGuinness L P, Plenio M B, Naydenov B, Jelezko F (2013) Detection of a few metallo-protein molecules using color centers in nanodiamonds. Nano Lett. 2013. 13, 3305-3309.
- 15. Huang T, Tzeng Y, Liu Y K, Chen Y C, Walker K R, Guntupalli R, Liu C (2004) Immobilization of antibodies and bacterial binding on nanodiamond and carbon nanotubes for biosensor applications. Diamond Relat. Mater. 2004. 13, 1098.
- Liu Y L ,Sun K W (2010) Protein functionalized nanodiamond arrays. Nanoscale Res. Lett. 2010.
 1045-1050.
- 17. Hubbell W L ,Altenbach C (1994) Investigation of structure and dynamics in membrane proteins using site-directed spin labeling. Curr. Opin. Struct. Biol. 1994. 4, 566-573.
- 18. Kao S C ,Bobst A M (2001) Local base dynamics and local structural features in RNA and DNA duplexes. Biochemistry. 2001. 24, 5465-5469.
- 19. Hubbell W L, Cafiso D S, Altenbach C (2000) Identifying conformational changes with site-directed spin labeling. Nat. Struct. Biol. 2000. 7, 735 739.
- 20. Edwards T E, Okonogi T M, Robinson B H, Sigurdsson S T (2001) Site-specific incorporation of nitroxide spin-labels into internal sites of the TAR RNA. Structure-dependent dynamics of RNA by EPR spectroscopy. J. Am. Chem. Soc. 2001. 123, 1527-1528.
- 21. O S, N P, J P, BE B, TF P, JW E (2007) Spin labeling of oligonucleotides with the nitroxide TPA and use of PELDOR, a pulse EPR method, to measure intramolecular distances. Nat. Protoc. 2007. 2, 904-923.
- 22. Hubbell W L, Mchaourab H S, Altenbach C, Lietzow M A (1996) Watching proteins using move using site-directed spin labeling. Structure. 1996. 4, 779-783.
- 23. Farahbakhsh Z T, Hideg K, Hubbell W (1993) Photoactived conformational changes in rhodopsin: A time-reolved spin label study. Science. 1993. 262, 1416-1419.

- 24. Steinhoff H-J, Mollaaghababa R, Altenbach C, Hideg K, Krebs M, Khorana H G, Hubbell W L (1994) Time-resolved detection of structure changes during the photocycle of spin-labeled bacteriorhodopsin. Science. 1994. 266, 105-107.
- 25. Stone K M, Voska J, Kinnebrew M, Pavlova A, Junk M J N, Han S (2013) Structural Insight into Proteorhodopsin Oligomers. Biophys. J. 2013. 104, 472-481.
- 26. Qin P Z, Haworth I S, Cai Q, Kusnetzow A K, Grant G P G, Price E A, Sowa G Z, Popova A, Herreros B, He H (2007) Measuring nanometer distances in nucleic acids using a sequence-independent nitroxide probe. Nat. Protoc. 2007. 2, 2354-2365.
- 27. Yamauchi J (2008) Molecular Magnetism, in handbook of Nitroxides: applications in chemistry, biomedicine, and materials science, Wiley-VCH, Weinheim, pp 47-68.
- 28. Romanova E E, Akiel R, Cho F H, Takahashi S (2013) Grafting nitroxide radicals on nanodiamond surface using click chemistry. J. Phys. Chem. A. 2013. 117, 11933–11939.
- 29. Akiel R, Zhang X, Abeywardana C, Stepanov V, Peter Z Qin, Takahashi S (2016) DNA barcoding of anodiamonds. 2016. submitted.
- 30. Cho F H, Stepanov V, Abeywardana C, Takahashi S (2015) 230/115 GHz electron paramagnetic resonance/double electron-electron resonance spectroscopy. Methods Enzymol. 2015. 95-118.
- 31. Cho F H, Stepanov V, Takahashi S (2014) A high-frequency electron paramagnetic resonance spectrometer for multi-dimensional, -frequency and -phase pulsed measurements. Rev. Sci. Instrum. 2014. 85, 42-55.
- 32. Xu J, Plaxco K W, Allen S J, Bjarnason J E, Brown E R (2007) 0.15–3.72 THz absorption of aqueous salts and saline solutions. Appl. Phys. Lett. 90. 2007. 90, 031908.
- 33. Barnes J P ,Freed J H (1997) Aqueous sample holders for high-frequency electron spin resonance. Rev. Sci. Instrum. 1997. 68, 2838-2846.
- 34. Polnaszek C F, Bruno G V, Freed J H (1973) ESR line shapes in the slow-motional region: anisotropic liquids. J. Chem. Phys. 1973. 58, 3185-3199
- Schneider D J ,Freed J H (1989) Spin relaxation and motional dynamics. Adv. Chem. Phys. 1989.
 73, 387-528.
- 36. Budil D E, Lee S, Saxena S, Freed J H (1996) Nonlinear-least-squares analysis of slow-sotion EPR spectra in one and two dimensions using a modified levenberg–marquardt algorithm. J. Magn. Reson. A. 1996. 120, 155-189
- 37. Schwartz L J, Stillman A E, Freed J H (1982) Analysis of electron spin echoes by spectral representation of the stochastic liouville equation. J. Chem. Phys. 1982. 77, 5410-5425.
- 38. Polimeno A ,Freed J H (1993) A many-body stochastic approach to rotational motions in liquids. Adv. Chem. Phys. 1993. 83, 89-206.

- 39. Zerbetto M, Polimeno A, Barone V (2009) Simulation of electron spin resonance spectroscopy in diverse environments: An integrated approach. Comput. Phys. Commun. 2009. 180, 2680.
- 40. Kimmich R (2012) Basic Phenomena and Definitions, in handbook of Principles of soft-matter dynamics: basic theories, non-invasive methods, mesoscopic aspects, Springer, Dordrecht, pp 1-87.
- 41. Stoll S ,Schweiger A (2006) EasySpin, a comprehensive software package for spectral simulation and analysis in EPR. J. Magn. Reson. A. 2006. 178, 42-55.